Int. J. Multiphase Flow Vol. 11, No. 2, pp. 241–254, 1985
Printed in the U.S.A.

0301-9322/85 $3.00 + .00
Pergamon/Elsevier

TRANSPORT PROCESSES IN FRACTALS

III. TAYLOR DISPERSION IN TWO EXAMPLES OF FRACTAL CAPILLARY NETWORKS

P. M. ADLER
Laboratoire d' Aérothermique, 4 ter, Route des Gardes, 92190-Meudon, France

(*Received* 20 *December* 1983; *in revised form* 23 *July* 1984)

Abstract—Taylor dispersion is studied on a tree and on a Sierpinski gasket. On a tree, the exact expression of the probability is obtained, from which the m-adic global moments are derived; various temporal behaviours are then exhibited, as they depend upon a geometrical parameter. On a Sierpinski gasket, numerical calculations are performed; the flow "field" is first discussed; Taylor dispersion is analysed with the help of the two first moments; the influence of the finite character of the network is clearly pointed out; the main conclusion is that Taylor dispersion is *almost completely independent* upon the flow field even for a low number of generations.

1. INTRODUCTION

Dispersion in cylindrical capillaries was first analysed by Taylor (1953); the moment-analysis technique was introduced by Aris (1956), and later on extended by Horn (1971). Finally, a general theory of dispersion in a spatially periodic porous medium was developed by Brenner (1980). Further progress was made when the porous medium can be schematized by a spatially periodic capillary network; a general formalism was introduced by Adler & Brenner (1984).

Meanwhile, fractal structures which are characterized by a dilational invariance (to be contrasted with the translational invariance of spatially periodic structures) were found to have a growing importance and many efforts have been recently devoted to them (see Mandelbrot 1982). In the previous issues of these series (Adler 1985a, 1985b), hereafter referred to as I and II, we studied the transport properties of a Leibniz packing, and the flow, in the stokes limit, in a general fractal capillary network.

The purpose of this paper is to prepare the general study of Taylor dispersion in a fractal capillary network by working out two simple and classical examples; the moments of the probability density will display an original behaviour. In spatially periodic structures, the two first moments of the probability density were found to be a linear and a square function of time, respectively. In the two examples, these moments display other time behaviours. Hence, this qualitative difference is very important and is expected to largely modify the mathematical background of the Taylor dispersion theory as it was set up for structures with a translational symmetry.

Some works can be cited in connection with fractal structures, since they are generally related to percolation networks; more precisely, the small-scale structure of the infinite cluster is self-similar. Sahimi *et al.* (1982) studied the dispersion in flow through porous media; they were mostly interested by the long-time behaviour when the dispersion is expected to present a diffusive character as a consequence of the translational symmetry at the large scale of the medium. A whole body of literature is concerned by random walks on fractals, with application of renormalization-group techniques (Gillies & Weiss 1970, Alexander *et al.* 1981, Alexander & Orbach 1982, and Sinai 1982) and by the so-called oriented conduction (see, for instance, Odagaki & Lax 1980). Of course, the present work is in many respects closely connected to them, but the essential difference is that the transfer rates are determined by the flow rates on the same network. Hence, in order to point out this specific feature, the present study is ranged in the class of Taylor dispersion phenomena.

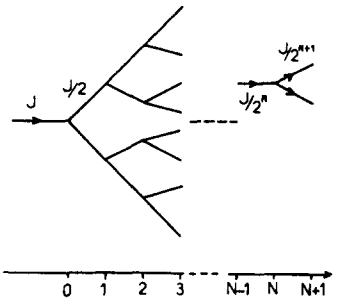

Figure 1. An infinite tree of degree 3.

This paper is organized as follows. The basic equations of Taylor dispersion are recalled in section 2. Then, the simplest example of a fractal structure, i.e. a tree, is analysed; the equations can be solved analytically and various time behaviours are obtained and discussed.

In section 4, the second example which is the Sierpinski gasket is studied. First, the flow rates along the edges are calculated as an application of the method derived in II; the geometry of these flow rates present some interesting features which are briefly mentioned, since it controls the dispersion through the network. Then, the probability densities are numerically calculated, and Taylor dispersion is analysed with the help of the two first moments. The finite character of the network disturbs the long-time behaviour of the moments; these unwanted effects are discussed in order to point out some of the universal characters of the results. The major conclusion of this preliminary study is that Taylor dispersion is very rapidly almost completely independent upon the flow field when the size of the network is increased.

Finally, a word of caution must be added here; some important questions are left unsolved and they may not have been put in the most convenient theoretical background. However, these two examples provided us with some useful hints for the development of a theory about Taylor dispersion in fractals, which would be at par with the development of Stokes flows in such networks.

2. BASIC EQUATIONS

A detailed presentation of the basic equations of Taylor dispersion in spatially periodic capillary networks is given by Brenner & Adler (1985). This presentation is briefly summed up and transposed to a fractal capillary network.

Let a fractal capillary network be represented by its graph Γ (see, for instance, the tree shown in figure 1). A fluid is assumed to flow through this network; generally, the vertices and the edges are numbered by the letters i and j, respectively. The flow rate along the edge j is denoted by $J(j)$.

Imagine a tracer particle initially introduced at time $t = 0$ into the network at vertex i'. The probability of finding this particle within any capillary will be assumed to be negligible owing to the relatively small volume assumed for the capillaries compared with the vertices. More precisely, the solute holdup within the capillaries is assumed negligible compared with its holdup in the "mixing chambers" represented by the vertices. The probability density of finding this tracer particle at vertex i at time t is denoted by

$$P(i, t \mid i'). \qquad [1]$$

When the capillary walls are assumed to be impermeable to solute permeation, the probability density at each vertex i obeys to the first-order differential equation

$$v(i) \cdot \frac{\mathrm{d}P(i, t \mid i')}{\mathrm{d}t} = \delta(i, i')\,\delta(t) + \sum_{j \in \Omega^+(i)} J(j)\,P(i'', t \mid i') - \left(\sum_{j \in \Omega^-(i)} J(j) \right) \cdot P(i, t \mid i'), \qquad [2]$$

where $\delta(i, i')$ is a Kronecker delta and $\delta(t)$ is a Dirac's delta function. $v(i)$ is the volume of vertex i. The edges j of the graph are oriented according to the flow rates along themselves; for a given vertex i, one can distinguish between the set $\Omega^+(i)$ of edges ending at i, and the set $\Omega^-(i)$ of edges beginning at i; when j belongs to $\Omega^+(i)$, it can also be denoted by $\{i'', i\}$.

The equation has already been commented on by Adler & Brenner (1984). The left-hand side represents the time rate of accumulation of the amount $v(i)P$ of solute contained in the vertex i. The first term on the right-hand side is a "source" term; the other terms describe the "convective" mass transfer occuring between connecting vertices. The essential assumption of perfectly mixing vertices is schematized by the fact that the pertinent flow rate is always weighted by the probability density of the vertex from which it comes. This assumed mixing property may be regarded as a consequence of one of several possible physical mechanisms. It may, for example, represent a strictly convective mixing process, such as occurs in a stirred tank. Alternatively, it may arise from intense molecular diffusion, considered to be dominant in the vertices—convection having previously been supposed dominant along the edges. Further commentary on these points was offered in Adler & Brenner (1984).

The probability also satisfies the usual unit normalization condition

$$\sum_{i \in V\Gamma} P(i, t \mid i')\, v(i) = 1, t > 0, \qquad [3]$$

where $V\Gamma$ is the vertex set of Γ.

The m-adic global moments of the probability density are defined by the expressions

$$\mathbf{M}_m(t \mid i') = \sum_{i \in V\Gamma} v(i)\, [\mathbf{R}(i) - \mathbf{R}(i')]^m P(i, t \mid i'), \qquad [4]$$

where, generically, for any vector $\mathbf{V}$, $\mathbf{V}^m$ is the m-adic $\mathbf{V}\,\mathbf{V} \ldots \mathbf{V}\,\mathbf{V}$ (m times). $\mathbf{R}(i)$ is the position vector of the vertex i.

Usually, only the two first moments are evaluated; the first one is related to the average translation of the tracer and the second one to its dispersion. In spatially periodic networks, in the asymptotic limit of long times, their time derivatives were found to be equivalent to

$$\frac{\mathrm{d}\,\mathbf{M}_1(t \mid i')}{\mathrm{d}t} \simeq \bar{\mathbf{v}}^*, \qquad [5a]$$

$$\frac{\mathrm{d}}{\mathrm{d}t} [\mathbf{M}_2(t \mid i') - \mathbf{M}_1(t \mid i')\, \mathbf{M}_1(t \mid i')] \simeq 2\, \bar{\mathbf{D}}^*, \qquad [5b]$$

where $\bar{\mathbf{v}}^*$ is equal to the interstitial velocity, and $\bar{\mathbf{D}}^*$ is the dispersivity dyadic.

Brenner (1980) and Adler & Brenner (1984) gave general methods to calculate these two quantities in spatially periodic porous media. Apart from the particular time dependency, we note that the time derivatives do not depend any more upon the initial vertex i', where the tracer was introduced.

In the following, we shall show that completely different features appear in Taylor dispersion on fractal structures.

3. TAYLOR DISPERSION ALONG A TREE

Generally speaking, a tree is a graph without any cycles (Biggs 1974). For sake of simplicity, we shall consider the simplest example of an infinite tree in which each vertex is connected to three other vertices. At each vertex, the graph is subdivided into two parts, as it is shown in figure 1.

Thus, at step N, we shall have 2^N vertices; it is assumed that the abscissa x_N of these 2^N vertices is equal to N

$$x_N = N. \tag{6}$$

The 2^N vertices at step N are assumed to have the same volume $v(N)$, which may be expressed as

$$v(N) = \left(\frac{\alpha}{2}\right)^N \tag{7}$$

in dimensionless units. α is an arbitrary constant which is assumed to be different than 1

$$\alpha \neq 1. \tag{8}$$

This restriction will be removed and discussed at the end of this section. Note that, for $\alpha = 2$, the volume of all the vertices is equal to 1; hence, at each step N, the volume offered to the fluid is multiplied by a factor 2. For $\alpha = 1$, the volume offered at each step is constant and equal to 1. For α smaller than 1, this total volume decreases.

The resistance to the flow is assumed to be the same for all the edges of the tree. Hence, starting at step $N = 0$ with a flow rate equal to J, the flow rate is equal to $J/2^N$ after N subdivisions, as it is illustrated in figure 1.

In order to keep simple notations and expressions, all the quantities introduced in this section are assumed to be dimensionless. Hence, in application of the general formula [2], the probability density $P(N, t)$ of any vertex of abscissa $N > 0$ satisfies the differential equation

$$\frac{\alpha^N}{J} \cdot \frac{\mathrm{d}P(N,t)}{\mathrm{d}t} = P(N-1,t) - P(N,t), \quad N \neq 0 \tag{9a}$$

$$\frac{1}{J} \cdot \frac{\mathrm{d}P(0,t)}{\mathrm{d}t} = -P(0,t), \quad N = 0. \tag{9b}$$

Imagine that a tracer particle is initially introduced at time $t = 0$ into the capillary network at position $R = 0$ (cf. figure 1); the corresponding initial conditions may be expressed as

$$P(0, t=0) = 1, \quad P(N, t=0) = 0, \quad N \neq 0. \tag{9c}$$

The general solution of this system can be derived by elementary means; the first values are equal to

$$\begin{aligned}
P(0,t) &= \mathrm{e}^{-Jt}, \\
P(1,t) &= \frac{1}{1-\alpha} \cdot (\mathrm{e}^{-Jt} - \mathrm{e}^{-(J/\alpha)t}), \\
P(2,t) &= \frac{1}{(1-\alpha)(1-\alpha^2)} \cdot (\mathrm{e}^{-Jt} - \mathrm{e}^{-(J/\alpha^2)t}) - \frac{1}{(1-\alpha)^2} \cdot (\mathrm{e}^{-(J/\alpha)t} - \mathrm{e}^{-(J/\alpha^2)t}), \\
&\vdots \\
P(N,t) &= \sum_{k=0}^{N} C_{N,k}\, \mathrm{e}^{-(J/\alpha^k)t},
\end{aligned} \tag{10}$$

where the constants $C_{N,k}$ are determined by [9]. It may be shown that they are given by

$$C_{0,0} = 1,$$
$$C_{N,N} = -\sum_{k=0}^{N-1} A(N-k,\alpha)\cdot C_{k,k}, \qquad [11]$$
$$C_{N,k} = A(N-k,\alpha)\cdot C_{k,k}, \quad k \leq N-1$$

where

$$A(l,\alpha) = \prod_{i=1}^{l} \frac{1}{1-\alpha^i}. \qquad [12]$$

These expressions are valid for $\alpha \neq 1$.

Introduction of [10] into [4] yields the following expression for the m-moment of the probability density

$$M_m(t \mid 0) = \sum_{N=0}^{\infty} N^m \cdot \alpha^N \cdot \left(\sum_{k=0}^{N} C_{N,k} \cdot e^{-(J/\alpha^k)t}\right). \qquad [13]$$

Let us now study the behaviour of these moments for the various ranges of variation of the geometric parameter, i.e. $\alpha > 1$, $\alpha < 1$ and $\alpha = 1$.

For $\alpha > 1$, the two first moments are illustrated in figure 2 for various values of α. Note, for instance, that the two first moments increase very slowly after some time. This is a consequence of the fact that the total space offered to the tracer particle is larger and larger, as it moves more and more slowly along the tree.

In this range of α, the limiting behaviour of $M_m(t \mid 0)$ at large times is *a priori* singular. Putting $t = \infty$ in the series [13] would yield the absurd result $M_m(t \mid 0) = 0$. The singular perturbation techniques employed by Cox & Brenner (1967) for another fluid-mechanics problem could be applied here; in essence, it consists of the splitting of the series into its inner and outer contributions.

An alternative way to obtain the result consists in considering the equivalent problem for large values of N. Then [9a] is equivalent to the convection equation

$$\frac{1}{J}\cdot\frac{\partial P}{\partial t} + \frac{1}{\alpha^x}\cdot\frac{\partial P}{\partial x} = 0. \qquad [14a]$$

When a particle is released at time $t = 0$, at $x = 0$, it will be found at time t at the position

$$x = \frac{\text{Log}\,(Jt\,\text{Log}\,\alpha + 1)}{\text{Log}\,\alpha}. \qquad [14b]$$

Hence, a logarithmic behaviour is expected for large values of time when α is larger than 1, for the first moment $M_1(t \mid 0)$.

Since no dispersion is associated with the convection equation [14a], the mean-square displacement $M_2(t \mid 0) - [M_1(t \mid 0)]^2$ is expected to be constant.

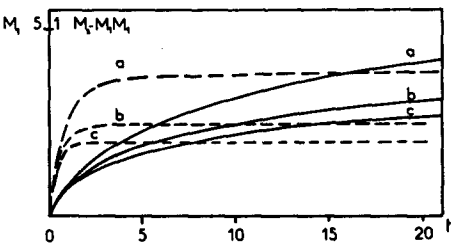

Figure 2. Taylor dispersion along a tree. Values of α are 2(a), 3(b), 4(c). The solid lines are for the first moment $M_1(t \mid 0)$, the broken lines for $M_2(t \mid 0) - M_1(t \mid 0)\,M_1(t \mid 0)$; note that the vertical scale is not the same for both quantities. The second quantity apparently reaches a constant value.

These two predictions are well verified by the numerical results illustrated in figure 2.

When α is strictly smaller than 1, a completely different qualitative behaviour happens, since less and less space is available to the tracer particle, as it proceeds in the tree. In this case, it is deduced from [14b] that the particle reaches infinity in a finite time t_0, which may be expressed as

$$t_0 = -\frac{1}{J \operatorname{Log} \alpha}, \quad \alpha < 1. \tag{15a}$$

After t_0, the amount of solute contained in the network at finite distances is smaller than 1. In the long-time limit, the probability density decays exponentially as

$$P(N, t) \simeq A(N, \alpha) \cdot e^{-Jt}. \tag{15b}$$

Introduction of [14] into [13] yields the following expression for the moments of the probability density

$$M_m(t \mid 0) \simeq \mathcal{M}_m \cdot e^{-Jt}, \tag{15c}$$

where $\mathcal{M}_m$ may be derived as

$$\mathcal{M}_m = \sum_{N=0}^{\infty} N^m \cdot \alpha^N \cdot A(N, \alpha). \tag{15d}$$

For sake of completeness, these two coefficients are displayed in table 1 for a few values of the parameter α. The divergence of $\mathcal{M}_m$ near 1 was not studied.

Table 1. The coefficients $\mathcal{M}_1$ and $\mathcal{M}_2$ as a function of α [see equations (15)]

α	$\mathcal{M}_1$	$\mathcal{M}_2$
0.05	0.058,332	0.064,486
0.10	0.137,44	0.168,24
0.15	0.245,86	0.334,17
0.20	0.396,84	0.601,16
0.25	0.611,58	1.0373
0.30	0.925,27	1.7669
0.35	1.3990	3.0273
0.40	2.4144	5.2984
0.45	3.3795	9.6197
0.50	5.5636	18.441
0.55	9.7655	38.180
0.60	18.805	88.109
0.65	41.478	237.61
0.67	59.974	374.90
0.69	90.141	617.71
0.71	141.96	1072.1

This exponential dependence of time is original in the Taylor dispersion context and it can be compared with [5]. The coefficients $\mathcal{M}_1$ and $\mathcal{M}_2$ do not depend upon the initial vertex through which the tracer particle was introduced into the network in contrast with e^{-Jt}. Clearly, if the tracer particle had been introduced into any vertex at step N, $M_1(t \mid N)$ and $M_2(t \mid N)$ would behave as

$$M_P(t \mid N) \simeq \mathcal{M}_P \cdot e^{-(J/2^N) \cdot t} \tag{16}$$

Let us investigate the last case $\alpha = 1$, which is very interesting since the exponential

dependence does not hold anymore. Equations [9] are replaced by

$$\frac{d}{dt} P(N, t) = P(N-1, t) - P(N, t), \quad N \neq 0 \tag{17a}$$

$$\frac{d}{dt} P(0, t) = -P(0, t), \quad N = 0 \tag{17b}$$

together with the initial conditions [9c]. The solution of this system is simply

$$P(N, t) = \frac{t^N}{N!} \cdot e^{-t} \tag{18}$$

since the forcing term has the same temporal behaviour as the solution of the homogeneous equation. Note that [18] is a Poisson distribution.

$M_1(t \mid 0)$ and $M_2(t \mid 0)$ are then easily deduced as

$$M_1(t \mid 0) = t, \tag{19a}$$

$$M_2(t \mid 0) = t^2 + t. \tag{19b}$$

The classical behaviour of Taylor dispersion in spatially periodic media is thus recovered (cf. [5]). It is, of course, a consequence of the fact that the total volume offered at each step is a constant.

4. TAYLOR DISPERSION ON A SIERPINSKI GASKET

This classical example of fractal is studied in this section. All edges are assumed to have the same resistance per unit length; the flow rates along the edges are calculated and their major features described and discussed. Then, Taylor dispersion is numerically studied; the influence of the hydrodynamic parameter λ, which controls the flows, is analyzed with a particular attention.

Flow rates along the edges

The Sierpinski gasket was studied in II and is illustrated in figure 3. The flow rates, which go out of the gasket Γ_N at step N, are denoted by $J_N^{(e)1}$, $J_N^{(e)2}$, $J_N^{(e)3}$; they are arbitrarily assumed to be positive when the flow goes out of Γ_N. They may be expressed as

$$\begin{aligned} J_N^{(e)1} &= -1, \\ J_N^{(e)2} &= \frac{1}{1+\lambda}, \\ J_N^{(e)3} &= \frac{\lambda}{1+\lambda}, \end{aligned} \tag{20}$$

where λ is a dimensionless parameter ranging from 0 to 1. In this section again, the flow rates, the time, . . . are assumed to be dimensionless for sake of simplicity.

Note in [20] that the sum of the three flow rates is equal to zero; the interval [0, 1] for λ is sufficient, since for λ larger than 1 the role of the two vertices $v_N^{(e)2}$ and $v_N^{(e)3}$ could be interchanged.

When the flow rates at the external vertices are known, it is a simple matter to calculate the flow rates on the various edges, by a repeated application of the matrix $\mathbf{H}_N$, introduced in II. The Sierpinski gasket of order N can be decomposed into three gaskets of order $N-1$.

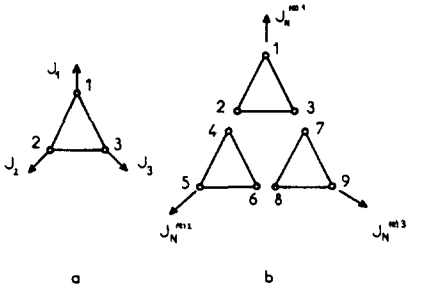

Figure 3. The construction process of the Sierpinski gasket. The basic graph Γ_0 is given in (a); 3 basic graphs are used to obtain the next generation as shown in (b).

The flow rates at the external vertices of the three gaskets of order $N-1$ can be related to the three external vertices of the overall gasket in the following way [with the notations of figure 3(b)]:

$$\begin{pmatrix} J_1 \\ J_2 \\ J_3 \\ J_4 \\ J_5 \\ J_6 \\ J_7 \\ J_8 \\ J_9 \end{pmatrix} = \frac{1}{3} \times \begin{pmatrix} 3 & 0 & 0 \\ -1 & 1 & 0 \\ -2 & -1 & 0 \\ 1 & -1 & 0 \\ 0 & +3 & 0 \\ -1 & -2 & 0 \\ 2 & 1 & 0 \\ 1 & 2 & 0 \\ -3 & -3 & 0 \end{pmatrix} \cdot \begin{pmatrix} J_1 \\ J_5 \\ J_9 \end{pmatrix}. \qquad [21]$$

Since the flow rate at the third external vertex is always equal to the opposite of the sum of the two other flow rates, it is sufficient to consider three 2×2 matrices

$$\begin{pmatrix} J_1 \\ J_2 \end{pmatrix} = \mathbf{A}_1 \cdot \begin{pmatrix} J_1 \\ J_5 \end{pmatrix}, \quad \begin{pmatrix} J_4 \\ J_5 \end{pmatrix} = \mathbf{A}_2 \cdot \begin{pmatrix} J_1 \\ J_5 \end{pmatrix}, \quad \begin{pmatrix} J_7 \\ J_8 \end{pmatrix} = \mathbf{A}_3 \cdot \begin{pmatrix} J_1 \\ J_5 \end{pmatrix}, \qquad [22]$$

where $\mathbf{A}_1$, $\mathbf{A}_2$ and $\mathbf{A}_3$ are readily deduced from [21].

These applications are easily implemented on a computer and an example is given in figure 4. The reader may check that the sum of the flow rates is equal to zero at each vertex and that the total pressure drop along every cycle of the graph vanishes identically.

It is interesting to consider the "streamlines" in the network, and they are represented for a few values of the parameter λ in figure 5. Let us focus our attention on the directions of the flow rates; these directions are important since they control the transfer by Taylor dispersion,

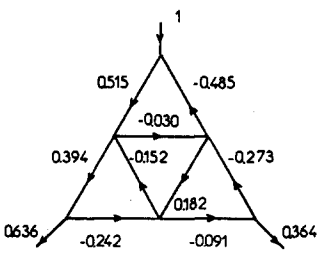

Figure 4. A numerical example of the flow rates along the edges of a Sierpinski gasket.

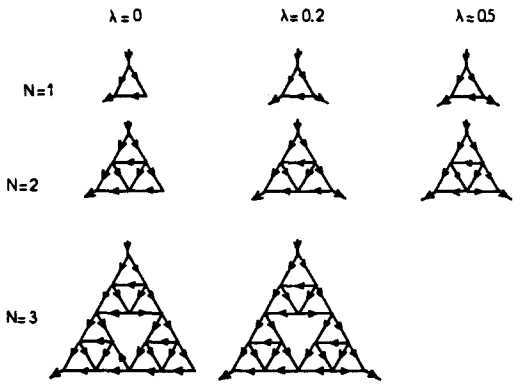

Figure 5. Directions of the flow rates along the edges of a Sierpinski gasket for various external flow conditions and various values of N.

as it follows from [2]. The signs are identical for the networks ($N = 1, \lambda = 0$) and ($N = 1$, $\lambda = 0.5$); then a difference appears at $N = 2$ for the same values of λ. Again, the signs are identical for the networks ($N = 2, \lambda = 0$) and ($N = 2, \lambda = 0.2$); a sign difference appears at $N = 3$.

Hence, the first rule seems clear. The signs on two finite networks can be made identical, by choosing two values of λ which are close enough. However, no matter how the two values of λ are close, one can find N large enough so that there exists at least one sign on the two networks which is different. Moreover, the differences between the signs is pushed forward, so to speak.

The other important feature is the fact that the numerical values of the flow rates in the inner structures tend towards a common limit when N increases; this limit does not depend upon λ. This is illustrated for the three first triangles in a network in table 2.

Table 2. Flow rates on the nine edges of the first three triangles as a function of the order N of the total gasket. The edge numbers are given in figure 6 together with their orientations

Edge	$N = 2$	$N = 3$	$N = 4$	$N = 5$
1	0.5556	0.5185	0.5062	0.5021
2	−0.1111	−0.0371	−0.0123	−0.0041
3	−0.4444	−0.4815	−0.4938	−0.4979
4	0.5556	0.4074	0.3580	0.3416
5	−0.4444	−0.2593	−0.1975	−0.1770
6	−0.1111	−0.1482	−0.1605	−0.1646
7	0.2222	0.1852	0.1728	0.1687
8	−0.1111	0.07407	0.1358	0.1564
9	−0.1111	−0.2593	−0.3086	−0.3251

The values of the flow rates at the external vertices of these three triangles are obtained by a multiplication by $\mathbf{A}_1 \cdot \mathbf{A}_1^n$ may be expressed as

$$\mathbf{A}_1^n = \begin{pmatrix} 1 & 0 \\ \dfrac{a_n}{3^n} & \dfrac{1}{3^n} \end{pmatrix}, \qquad [23]$$

where $a_{n+1} = 3a_n - 1$ and $a_1 = -1$.

For n large, $\mathbf{A}_1^n$ becomes equivalent to

$$\mathbf{A}_1^n = \begin{pmatrix} 1 & 0 \\ -\dfrac{1}{2} & 0 \end{pmatrix}, \quad n \text{ large.}$$

Hence, the flow rates do not depend anymore on J_5, and thus they are independent of the flow parameter λ.

It may be said that there is a kind of isotropisation, since the anisotropy induced by λ is quickly forgotten in the inner structures. Such a phenomenon has already been encountered in I; an anisotropic Leibniz packing was shown to give the same results for the conduction process as an isotropic packing.

Finally, in consequence of this isotropisation, it may be expected that Taylor dispersion does not depend too much upon the flow parameter λ.

Taylor dispersion

The present situation differs from the previous one in a tree. The differential system [2] cannot be solved analytically, since the network contains cycles.

Hence, the system [2] was solved numerically for finite networks. The algebraic value of the flow rates along the edges of the network is first calculated; then, the set $\Omega^+(i)$ and $\Omega^-(i)$ are automatically determined for each vertex inside the network. The differential system [2] is calculated and is integrated with the aid of a subroutine which belongs to the IMSL Library. Various tests of accuracy and self-consistency were performed on the results.

Of course, the larger is the network, the larger is the differential system to solve. It was experimentally found that most of the interesting features were displayed with 27 triangles corresponding to a gasket of order 4. This gasket is given in figure 6 with some notations such as the numbering of the vertices. This amounts to the simultaneous resolution of 42 differential equations.

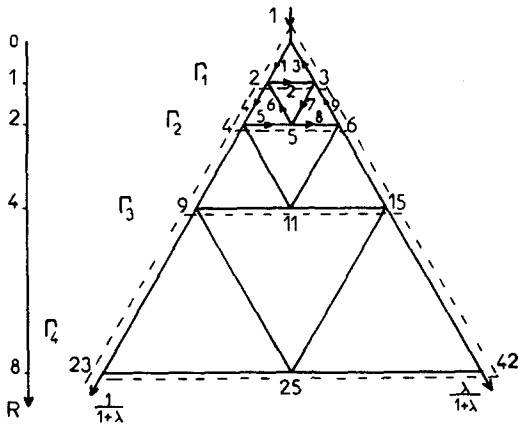

Figure 6. The Sierpinski gasket of 27 triangles ($N = 4$), on which the numerical calculations were performed. Some relevant vertex numbers are given. The abscissae of the vertices is shown by the vertical scale on the left. Light broken lines are used to indicate the subgraphs Γ_1, Γ_2 and Γ_3.

The vertices are assumed to have the same volume 1, and they are regularly spaced. The abscissa of the vertex i along the R axis (cf. figure 6) is denoted by $R(i)$; for instance, $R(1)$, $R(2)$, $R(4)$ and $R(9)$ are equal to 0, 1, 2 and 4, respectively. These simple hypotheses may, of course, be modified in future works. The tracer particle is always introduced at vertex 1 at time $t = 0$, according to [2]. For such a finite network, the particle is of course allowed to leave the network at vertices 23 and 42. Hence, the total amount of solute decreases with time in contradiction with equations [3]. In order to take this fact into account, the expressions [4] of the m-adic global moments are here modified as

$$M'_m(t \mid 0) = \frac{M_m(t \mid 0)}{M_0(t \mid 0)}, \quad m \geq 1. \qquad [24]$$

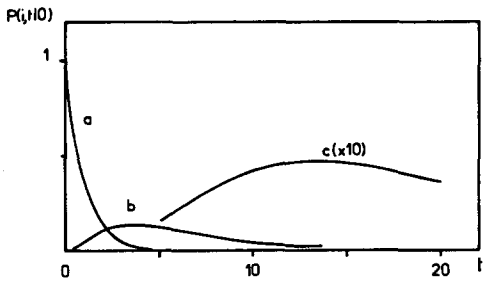

Figure 7. Evolution of the probability density as a function of time for three vertices. The number of the vertices are 1(a), 5(b), 11(c); their location is given in figure 6. λ is equal to 1.

Besides these quantities, it was found useful to analyse moments of the probability density evaluated on subunits of the complete network. We define three additional m-adic global moments by

$$M'^{j}_{m}(t \mid 0) = \frac{\sum_{i \in V\Gamma_j} [R(i)]^m \cdot P(i, t \mid 0)}{\sum_{i \in V\Gamma_j} P(i, r \mid 0)}, \qquad [25]$$

where j varies from 1 to 4. Γ_1 consists of the first triangle, Γ_2 of the first three triangles, Γ_3 of the first nine triangles and Γ_4 of the first twenty-seven triangles (i.e. of the whole network); this is illustrated in figure 6. Note that $M'^{4}_{m}(t \mid 0)$ and $M'_{m}(t \mid 0)$ are identical.

In principle, the various moments of the probability distributions are m-order tensors (cf. [4]). Here, we restricted ourselves to their values along the R axis. This is due to the fact that the gasket is limited in its lateral direction (say y) perpendicular to the R-axis; hence, one will see mostly the influence of this geometrical limitation in the results. Note also, in view of the geometrical symmetry, that the first lateral moment is equal to zero for a large number of triangles.

Numerical results are now displayed in a series of figures and commented. In order to further check the numerics, the evolution of the probability density in a few arbitrary vertices is presented in figure 7. Two important features are obtained. First, the various maxima are shifted in time one with respect to the other one, which corresponds to the "passage" of the tracer particle; second, the maximum in time of the probability density goes to zero very rapidly, since more and more space is available to the tracer particle as it proceeds along the structure.

The evolution in time of the total amount of solute inside the various graphs Γ_j is shown in figure 8 for a given value of the hydrodynamic parameter λ. It will be shown later that this result is remarkably insensitive to λ. The various amounts of matter $M'_0(t \mid 0)$ decrease with time as expected. There is no obvious time scaling relation between these various quantities.

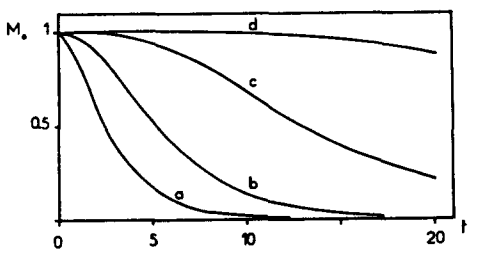

Figure 8. Evolution of the amount of solute $M'_0(t \mid 0)$ for the various subgraphs Γ_j. λ is equal to 1. Values of j are 1(a), 2(b), 3(c), 4(d).

Stopping times $t^j_{p_0}$ could be defined from these curves in the following way: $t^j_{p_0}$ is the time at which an amount P_0 of matter stays in the subunit Γ_j. An example deduced from figure 8 could be for P_0 equal to 0.1

$$t^j_{0.1} = 6.00,\ 11.0,\ 25.9,\ 70.8 \text{ for } j = 1,2,3,4.$$

Again there is no obvious scaling, but the relation between the various stopping times is highly nonlinear. The larger the network, the longer it retains the tracer particle. This is consistent with the fact that the maximum in the probability density in time is smoother as we proceed along the structure (it is illustrated in figure 7).

The evolution in time of the first moments on the various graphs Γ_j is shown in figure 9 for a given value of the hydrodynamic parameter λ. It is only the first part of each curve which is interesting. Actually each curve is superposed for sufficiently short times with the universal curve corresponding to an infinite network. Note that most of the matter is still contained inside Γ_4 at time $t = 10$ (cf. figure 8); hence, it is expected that $M^{\Gamma_4}_1(t \mid 0)$, obtained for Γ_4, is a good approximation of $M_1(t \mid 0)$ in an infinite network for times lower than 10.

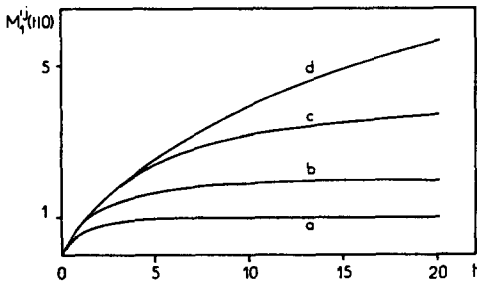

Figure 9. Evolution of the position of the center of gravity $M^j_1(t \mid 0)$ for the various subgraphs Γ_j. λ is equal to 1. Values of j are 1(a), 2(b), 3(c), 4(d).

The saturation of $M^{j'}_1(t \mid 0)$ at large times is largely irrelevant; it is related to the fact that most of the solute is concentrated at the end of the submit for large times; hence, $M^{j'}_1(t \mid 0)$ is equal to the largest abscissa of the vertices which belong to Γ_j.

Finally, it should be noticed that the maximum in the local probability density shown in figure 7 is roughly obtained when $M'_1(t \mid 0)$ is equal to the abscissa of the vertex under consideration.

Dispersion is represented in figure 10. Comments very similar to the ones made for $M^{j'}_1(t \mid 0)$ can be given. Again, only the first part of the curves is interesting, since it is related to the dispersion in an infinite network. Using the same argument as before, the dispersion in an infinite network can certainly be well approximated for $t \ll 10$ by the curve relative to Γ_4. The decreasing part of the curves is simply caused by the finite character of the network; when matter leaves the network, it contributes to the reduction of the dispersion.

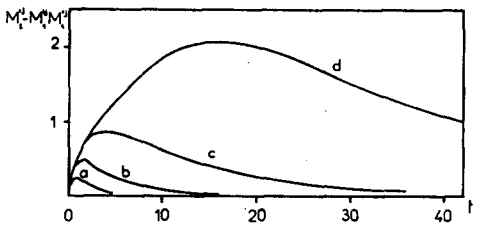

Figure 10. Evolution of the dispersion $M^j_2(t \mid 0) - [M^j_1(t \mid 0)]^2$ for the various subgraphs Γ_j. λ is equal to 1. Values of j are 1(a), 2(b), 3(c), 4(d).

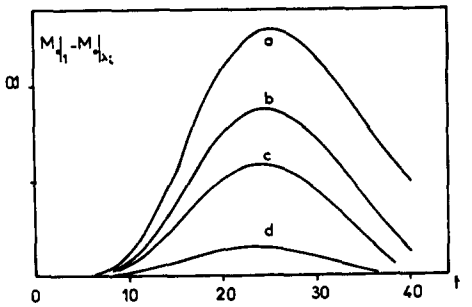

Figure 11. Evolution of the difference $M_0(t \mid 0)|_{\lambda=1} - M_0(t \mid 0)|_{\lambda_i}$. Values of λ_i are 0(a), 0.1(b), 0.2(c), 0.5(d). These differences are evaluated on Γ_4.

Let us finally investigate the influence of the hydrodynamic parameter λ. This is illustrated in figure 11 for the difference between probabilities, with a large vertical scale. Generally, this difference presents an oscillatory behaviour which is damped in time; however, it was not found necessary to display this long-time behaviour. As it was expected, the largest difference was numerically found to occur between the two extreme situations $\lambda = 0$ and 1; note that the maximum does not exceed 13%, which is already pretty small in view of the differences between these two hydrodynamic situations. An other interesting feature is that the value of the maximum decreases very rapidly when λ increases; the difference becomes relatively significant only when extreme situations are considered.

This very important result can be explained with the aid of the preliminaries developed for the flow rates. It was shown that the flow rates in the subgraphs Γ_j were only slightly dependent upon the flow parameter λ (cf. table 2); for 27 triangles the dependence of the inner structures was already very small. By its very nature, the Taylor dispersion tends to damp these differences, since it is a mixing process.

Another test of the influence of λ was made. The network Γ_4 was imbedded in a network Γ_5; the flow rates were measured at the end vertices of Γ_5. The probability density was calculated as before inside Γ_4. It was numerically shown that the maximum density difference was lower than 1.5% for the two extreme situations at the end vertices of Γ_5. Hence, the influence of the flow parameter becomes rapidly negligible.

This feature could be further investigated by considering the reduction of triangles . . ., however, at the stage of the present study, we are mostly concerned by the extension of the results to a very large network. Note in this respect that the numerical results were all given for $\lambda = 1$, which is very close to the final situation in an infinite network.

Finally, we may conclude on the large time behaviour of the various moments of the distributions. In view of what happened along a tree with $\alpha > 1$, a similar behaviour may be expected since the volume offered to the tracer particle is an increasing function of R; however, the Sierpinski gasket is characterized by the regular presence of bottlenecks, such as the vertices 9 and 15 (see figure 6) between Γ_3 and Γ_4. The passage of the tracer particle through these bottlenecks may thus profoundly alter the large-time behaviour of the various moments.

5. CONCLUDING REMARKS

As it was said at the beginning, this paper should be considered as a mere introduction to the general study of Taylor dispersion in fractal capillary networks.

These preliminary numerical results pointed out some problems to be solved in a general framework. For instance, the essential question of the behaviour at large times was only touched upon in section 3 where analytic expressions could be obtained. When such analytic expressions are not available, the question is to find recursive relations between successive generations of fractals inside which convection and Taylor dispersion occur.

Another interesting problem is the embedding of finite fractals in spatially periodic structures and the related calculations of the homogenous dispersion dyadic (see II for the derivation of the permeability).

Finally, the extension to continuous situations has to be considered. For instance, the calculation of Taylor dispersion inside a Leibniz packing could provide a first example (see I).

Acknowledgements—The author gratefully acknowledges stimulating comments of the referees. This work was partly supported by a C.N.R.S. grant (A.T.P. from P.I.R.M.A.T. 11).

REFERENCES

ADLER, P. M. 1985a Transport processes in fractals. I. Conductivity and permeability of a Leibniz packing in the lubrication limit. *Int. J. Multiphase Flow* **11**(1), 91–108.

ADLER, P. M. 1985b Transport processes in fractals. II. Stokes flow in fractal capillary networks. *Int. J. Multiphase Flow* **11**(2), 213–239.

ADLER, P. M. & BRENNER, H. 1984 Transport processes in spatially periodic capillary networks. II. Taylor dispersion with mixing vertices. *Physico Chem. Hydro.*, **5**, 269–85.

ALEXANDER, S., BERNASCONI, J., SCHNEIDER, W. R. & ORBACH, R. 1981 Excitations dynamics in random one-dimensional systems. *Rev. Mod. Phys.* **53**, 175–98.

ALEXANDER, S. & ORBACH, R. 1982 Density of states on fractals: "fractons." *J. Phys. Lett.* **43**, L625–31.

ARIS, R. 1956 On the dispersion of a solute in a fluid flowing through a tube. *Proc. R. Soc. Lond.* **A235**, 67–77.

BIGGS, N. 1974. *Algebraic graph theory*. Cambridge University Press.

BRENNER, H. 1980. Dispersion resulting from flow through spatially periodic porous media, Phil. *Trans. Roy. Soc. London* **A297**, 81–133.

BRENNER, H. & ADLER, P. M. 1985 Transport processes in porous media. Hemisphere/ McGraw-Hill, New York.

COX, R. G. & BRENNER, H. 1967 The slow motion of a sphere through a viscous fluid towards a plane surface. II. Small gap widths, including viscous effects. *Chem. Engng. Sci.* **21**, 1753–77.

GEFEN, Y., AHARONY, A. & ALEXANDER, S. 1983 Anomalous diffusion on percolating clusters. *Phys. Rev. Lett.* **50**, 77–80.

GILLIS, J. E. & WEISS, G. H. 1970 Expected number of distinct sites visited by a random walk with an infinite variance. *J. Math. Phys.* **11**, 1307–12.

HORN, F. J. M. 1971 Calculation of dispersion coefficients by means of moments. *Aiche J.* **17**, 613–20.

MANDELBROT, B. B. 1982 *The fractal geometry of nature*. Freeman, San Francisco.

ODAGAKI, T. & LAX, M. 1980 A.C. Hopping conductivity of a one-dimensional bond-percolation model. *Phys. Rev. Lett.* **45**, 847–50.

SAHIMI, M., HEIBA, A. A., HUGHES, B. D., DAVIS, H. T. & SCRIVEN, L. E. 1982 Dispersion in flow through porous media, SPE 10969 Soc. Petrol. Engrs, New-Orleans, Louisiana 70 pp.

SINAI, YA. G. 1982 The limiting behaviour of a one-dimensional random walk in a random medium. *Theory Prob. Appl.* **27**, 256–68.

TAYLOR, G. I. 1953 Dispersion of soluble matter in solvent flowing slowly through a tube. *Proc. Roy. Soc. London* **A219**, 186–203.